Bioorganic Chemistry 161 (2025) 108507

Contents lists available at ScienceDirect

Bioorganic Chemistry

journal homepage: www.elsevier.com/locate/bioorg

Designing novel tridentate iridium(III) complexes comprising functionalized benzothiazole ligands to improve anticancer activity by targeting mitochondria☆

Qin Zhou [a,c], Xiao-Bin Zhang [a], An-Li Liu [a,c], Zhi-Gang Niu [a,c,*], Gao-Nan Li [a,c,*], Fa-Biao Yu [b,c]

[a] Key Laboratory of Electrochemical Energy Storage and Light Energy Conversion Matreials of Haikou City, Key Laboratory of Electrochemical Energy Storage and Energy Conversion of Hainan Province, College of Chemistry and Chemical Engineering, Hainan Normal University, Haikou 571158, China
[b] Key Laboratory of Emergency and Trauma, Ministry of Education, Key Laboratory of Haikou Trauma, Key Laboratory of Hainan Trauma and Disaster Rescue, The First Affiliated Hospital, Hainan Medical University, Haikou 571199, China
[c] Engineering Research Center for Hainan Bio-Smart Materials and Bio-Medical Devices, Key Laboratory of Hainan Functional Materials and Molecular Imaging, College of Emergency and Trauma, Hainan Medical University, Haikou 571199, China

ARTICLE INFO

Keywords:
Iridium (III) complex
Tridentate ligands
Benzothiazole
Anticancer
Mitochondria

ABSTRACT

In recent years, organo-iridium anticancer agents have shown promising antitumor activity toward cancer cells. In this paper, two benzothiazole-based tridentate ligands, 2,2′-(5-(*tert*-butyl)-1,3-phenylene)bis(benzo[*d*]thiazole) (**L_1**) and 2,2′-(5-(methyl)-1,3-phenylene)bis(benzo[*d*]thiazole) (**L_2**), have been designed and synthesized, and then combined with 2,2′-bipyridine (bipy) and 1,10-phenanthroline (phen) ancillary ligands to form a series of novel $[Ir(N^{\wedge}C^{\wedge}N)(N^{\wedge}N)Cl]^{+}$-type iridium(III) complexes (**Ir1**-**Ir4**). The phosphorescence properties of these complexes facilitate the visualization of their subcellular localization and interactions with other biomolecules. Among them, complex **Ir2** has the best cytotoxicity activity toward A549 cells and its antitumor activity was further evaluated. Laser confocal assay reveals that **Ir2** followed an energy-dependent cellular uptake mechanism and specifically accumulates in mitochondria (Pearson colocalization coefficient: 0.89). The anticancer mechanism has been explored through apoptosis, cell cycle arrest, western blotting (WB), reactive oxygen species (ROS) levels and mitochondrial membrane potential (MMP) changes. The antitumor activity *in vivo* confirms that **Ir2** could effectively inhibit tumor growth with an inhibitory rate of 71.60 %, which is superior to cisplatin. To the best of our knowledge, **Ir2** is a rare example of $[Ir(N^{\wedge}C^{\wedge}N)(N^{\wedge}N)Cl]^{+}$-type complexes as potential anticancer agents.

1. Introduction

Cancer is a malignant disease threatening human health and life due to its excessive proliferation, easily dispersed and transported characteristics [1–3]. Chemotherapy based on metal-organic medications is one of the most prevalent methods in cancer treatment [4,5]. At present, platinum drugs represented by cisplatin have proven to be effective chemotherapeutic agents against various types of cancers [6–8]. With the widespread use of cisplatin in clinical practice, however, some drawbacks are gradually found, such as drug resistance, high toxicity and serious side effects [9,10]. Therefore, a large of efforts have been made to explore different anticancer metal complexes as alternative of cisplatin, involving iridium [11], rhenium [12], gallium [13], gold [14], ruthenium [15], copper [16], rhodium [17] and more. Among them, organometallic Ir(III) complexes as potential anticancer agents have been studied extensively in recent years, because of their rich photophysical properties, good biocompatibility and excellent anticancer activities [18–22].

Based on different ligands, iridium(III) anticancer complexes are mainly classified into four types: cyclopentadienyl [23–25],

☆ This article is part of a Special issue entitled: 'Targeted cancer therapy' published in Bioorganic Chemistry.

* Corresponding authors at: Key Laboratory of Electrochemical Energy Storage and Light Energy Conversion Matreials of Haikou City, Key Laboratory of Electrochemical Energy Storage and Energy Conversion of Hainan Province, College of Chemistry and Chemical Engineering, Hainan Normal University, Haikou 571158, China.
E-mail addresses: niuzhigang1982@126.com (Z.-G. Niu), ligaonan2008@163.com (G.-N. Li).

https://doi.org/10.1016/j.bioorg.2025.108507
Received 8 March 2025; Received in revised form 11 April 2025; Accepted 21 April 2025
Available online 22 April 2025

cyclometalated [26–28], arene [29] and carbene [30–32]. By comparison, cyclometalated Ir(III) complexes possess easier adjustment in structure owing to great diversity of coordinating ligands. As such, these complexes can be precisely structurally modulated through introducing biomolecular functional groups on ligands, with the aim of effectively regulating their cytotoxic profiles and anticancer activities [33]. Lu et al. reported two sulfur-coordinated organoiridium(III) complexes (pbtIrSS and ppyIrSS) with C,N and S,S (dithione) chelating ligands, which inhibit breast cancer tumorigenesis and metastasis by blocking Wnt/β-catenin signaling cascade [34]. Mao et al. developed two iridium(III)-tripenylamine photosensitizers (IrC and IrF), representing the first integration of pyroptosis and ferroptosis hybrid cell death induction through disrupting redox balance and inducing photo-driven DNA and KEAP1 cascade damage [35]. Chao et al. reported an iridium(III) complex containing the derivate bis(2-chloroethyl)-azane, which localized in the ER and induced ICD in non-small-cell lung cancer [36].

So far, numerous bis/tri-cyclometalated Ir(III) complexes with bidentate ligands have been designed and prepared, and structure-activity relationships have also been established [37–39]. Nevertheless, it is worth mentioning that the exploration of tridentate Ir(III) complexes is an area that remains relatively scarce. Though there have been a few recent reports of these complexes for biological applications, the cases are only limited to $[Ir(N^{\wedge}N^{\wedge}N)(C^{\wedge}N)Cl]^{+}$ [40,41], $[Ir(N^{\wedge}N^{\wedge}N)(C^{\wedge}N^{\wedge}C)]^{+}$ [42], $[Ir(N^{\wedge}N^{\wedge}N)_2]^{3+}$ [43] and dinuclear Ir(III) complexes with tridentate ligands [44,45]. It is thus to be motivated to develop new types of tridentate ligand incorporating special functional group to apply in the area of iridium-based anticancer therapeutic agents.

As well known, benzothiazole contains a benzene ring fused to a thiazole ring, displaying remarkable biological properties, especially high anticancer activity [46,47]. In the past three decades, a great deal of research groups have been devoted to develop effective anticancer drugs with benzothiazole derivatives [48,49]. In addition, conventional 2,2′-bipyridine (bipy) and 1,10-phenanthroline (phen) ligands possess high lipophilicity, which help to enhance the biocompatibility of complexes through facilitating the cellular uptake and accumulation [50–52]. Based on above considerations, we introduced functionalized benzothiazole group onto the tridentate ligand to improve anticancer activity of corresponding Ir(III) complexes, and thus designed two novel ligands 2,2′-(5-*(tert*-butyl)-1,3-phenylene)bis(benzo[*d*]thiazole) (**L_1**) and 2,2′-(5-(methyl)-1,3-phenylene)bis(benzo[*d*]thiazole) (**L_2**), and then combined bipy and phen ancillary ligands to obtain a series of new type $[Ir(N^{\wedge}C^{\wedge}N)(N^{\wedge}N)Cl]^{+}$ complexes (**Ir1**-**Ir4**, Scheme 1). The structure of complex **Ir1** was studied by X-ray crystallography (Fig. 1). Their photophysical properties and cytotoxic profiles were investigated systematically. It was determined that complex **Ir2** had good fluorescence imaging capability and remarkable cytotoxicity to A549 cells. Subsequently, the anticancer mechanism *in vitro* and anticancer effects *in vivo* of **Ir2** were discussed and evaluated, respectively. As a result, our findings demonstrated that complex **Ir2** could induce the apoptosis of A549 cells by activating mitochondria apoptotic pathway of ROS and MMP regulated dysfunction. Furthermore, antitumor assays in nude mice showed **Ir2** could significantly prevent tumor growth *in vivo*, indicating its potential as novel anticancer drugs.

2. Results and discussion

2.1. Synthesis and characterization

As shown in Scheme 1, the cyclometalated N^C^N ligands (**L_1** and **L_2**) were prepared in good yields from ring condensation reactions between 2-aminothiophenol and 5-*tert*-butylisophthalic acid/5-methylisophthalic acid. Next, the two ligands reacted with $IrCl_3{\cdot}3H_2O$ to generate the corresponding chloro-bridged dimers, and then N^N ligands (bipy or phen) and silver trifluoromethyl sulfonate ($Ag(CF_3SO_3)$) were added into the reaction system to form the target Ir(III) complexes in moderate yields [53]. The structures of these compounds and

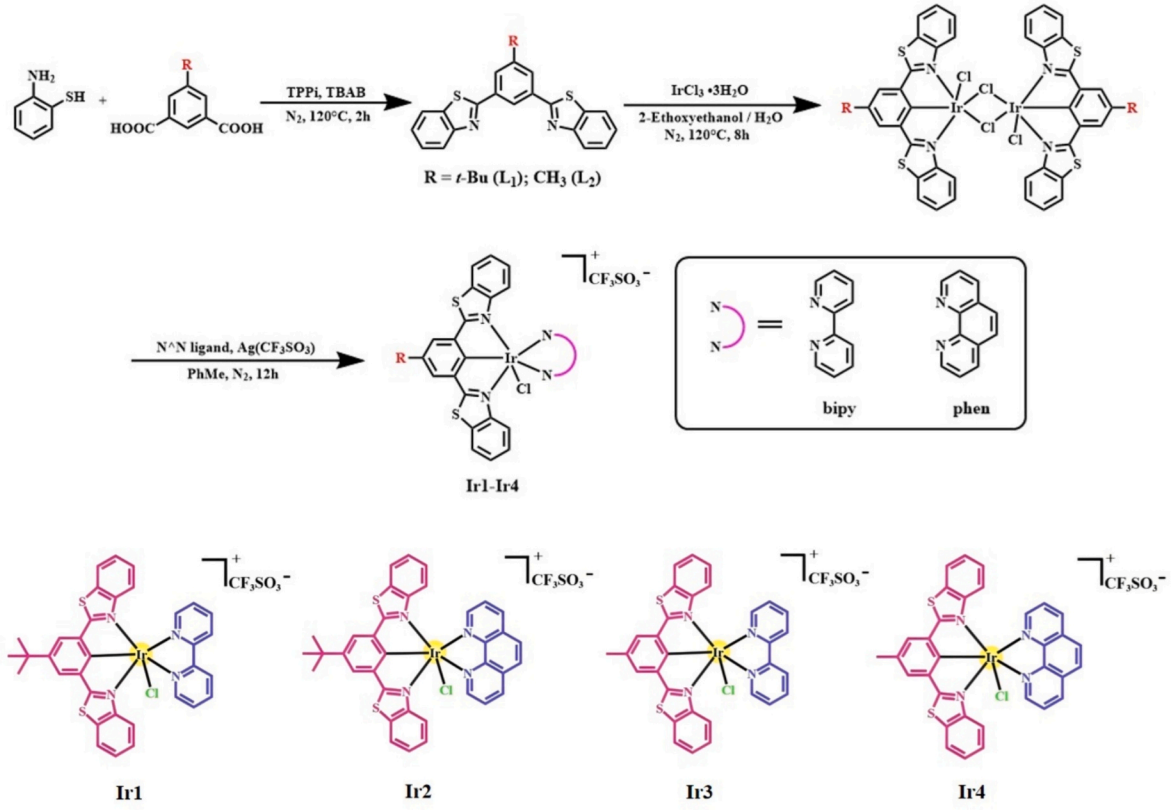

Scheme 1. The synthetic routes of complexes **Ir1**-**Ir4**.

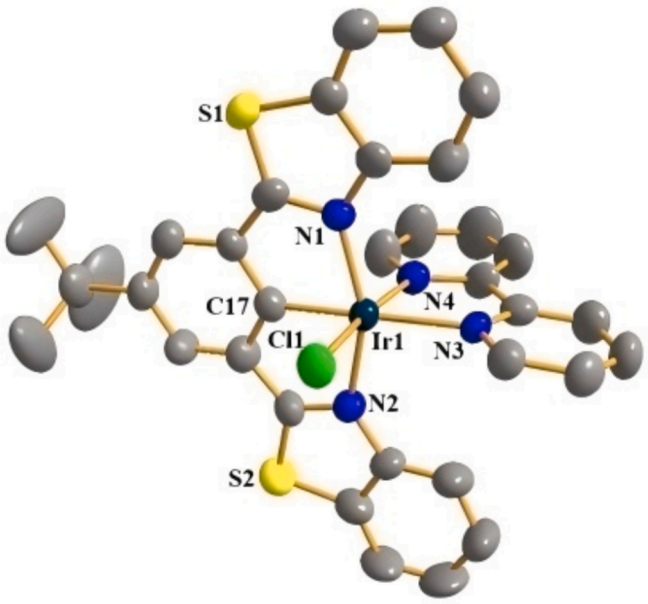

Fig. 1. Crystal structure of complex **Ir1** (CCDC: 2327299). For clarity, hydrogen atoms and the counter anion are omitted.

complexes were characterized by ^{1}H NMR (Figs. S6-S11), ^{13}C NMR (Figs. S12-S15), high-resolution mass spectrometry (HRMS) (Figs. S16-S21) and elemental analysis, as well as **Ir1** by X-ray single structure analysis (Fig. 1 and Tables S1-S2).

Single crystals of complex **Ir1** were obtained by slowly evaporating from the mixed dichloromethane and methanol solution at room temperature. The molecular structure with the cationic part is shown in Fig. 1. The crystallographic data and selected bond lengths/angles around the iridium center are listed in Tables S1-S2. The Ir(III) center presents a distorted octahedral coordination geometry with N1/N2/C17 atoms of $\mathbf{L_1}$ ligand, N3/N4 atoms of bipy ligand and monodentate chloride ligand. The N1/N2/C17 atoms are in a meridional arrangement, and nearly coplanar with the N3 atom with the average deviation from a least-squares plane of 0.0427 Å. The chloride ligand is in a position *trans* to the N4 atom and the length of the Ir—Cl bond (2.3481(15) Å) is much longer than those of other coordination bonds, as previously reported iridium analogues [54,55]. Moreover, Ir—Cl bond is almost perpendicular to the N1/N2/C17/N3 plane with bond angles of 88.87 (14)-93.73(13)°. The chelating C-Ir-N (N^C^N) and N-Ir-N (N^N) angles are around 78° while the *trans* N-Ir-N, C-Ir-N and Cl-Ir-N angles are in the range of 157.68(18)°-175.2(2)°.

2.2. Photophysical properties

The UV–vis and emission spectra of **Ir1**-**Ir4** in CH_2Cl_2 at 298 K are depicted in Fig. 2 and the corresponding data are given in Table S3. As shown in Fig. 2a, all complexes exhibit a strong absorption band (220–350 nm) and a weak absorption band (350–500 nm), which are attributed to spin-allowed ligand-centered (^{1}LC) π-π* transitions and an admixture of metal-to-ligand/intraligand/ligand-to-ligand charge transfer (MLCT/ILCT/LLCT) transitions, respectively [56,57]. Through the DFT calculation results, the lower-lying absorption of all Ir(III) complexes are associated with HOMO→LUMO+1 transitions (Table S4). From Table S5, the HOMOs mainly reside on the Ir (29.87–30.43 %, **Ir1**-**Ir4**) and N^C^N ligands (60.29–61.62 %, **Ir1**-**Ir4**), while the LUMO+1 s are mainly located on the N^C^N ligands (97.44 %, **Ir1**; 66.60 %, **Ir2**; 97.29 %, **Ir3**; 69.94 %, **Ir4**) and N^N ligands (31.42 %, **Ir2**; 28.00 %, **Ir4**). Therefore, the lowest energy bands mainly arise from MLCT/ILCT transitions ($d\pi_{Ir/N^C^N} \rightarrow \pi^*_{N^C^N}$, **Ir1** and **Ir3**) and MLCT/ILCT/LLCT transitions ($d\pi_{Ir/N^C^N} \rightarrow \pi^*_{N^C^N/N^N}$, **Ir2** and **Ir4**), further supporting the above description. There are no distinct differences on the absorption edge of complexes **Ir1**-**Ir4**, in line with the approximate energy gaps based on the DFT calculations (Fig. 3). It can be also found that iridium complexes with the same N^N ligand, **Ir1**/**Ir3** and **Ir2**/**Ir4**, have similar UV spectral profiles. The observation clearly demonstrates that the N^C^N ligand modifications (*t*-Bu and CH_3) have a negligible impact on the absorption spectra.

Upon photoexcitation, complexes **Ir1**-**Ir4** showed yellow-green phosphorescence (photos in Scheme S1 and CIE data in Table S3) with emission maximum peaking at ≈540 nm (Fig. 2b). The vibronic-structured emission bands reveal that their emissive excited states originate from the combined ^{3}MLCT and ^{3}LC characteristics [58,59]. In those analogues, the HOMO-1 s involve Ir metal and the N^C^N ligand, while the LUMO+1 s primarily reside on the N^C^N ligand (**Ir1** and **Ir3**) or the N^C^N/N^N ligands (**Ir2** and **Ir4**). So, the lowest-lying triplet states (T_1) based on HOMO-1 → LUMO+1 orbital transition exhibit the mixed characteristics of MLCT/ILCT for **Ir1** and **Ir3** or MLCT/ILCT/LLCT for **Ir2** and **Ir4** (Table S4). The calculated results agree well with the structured emission profiles, as well as their low-energy absorption transitions. Besides, the difference in peak wavelength turns evidently small among the four complexes, implying that the changes of main and ancillary ligands seem to not affect their emission spectra. The phosphorescence relative quantum yields (Φ_{em}) of **Ir1**-**Ir4** in dichloromethane solutions were measured to be 15.1–54.6 %, with lifetimes in

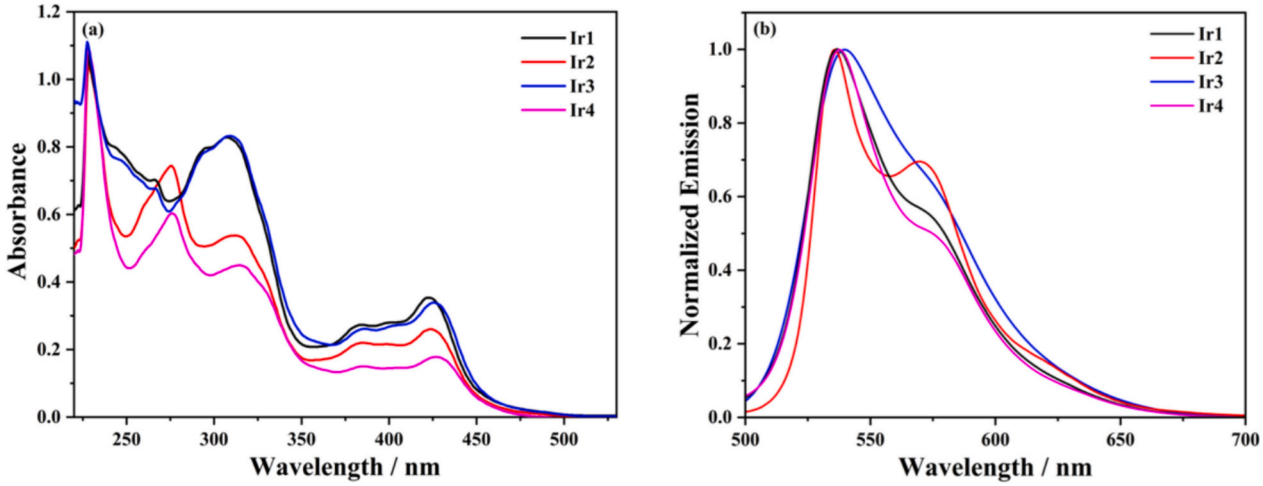

Fig. 2. UV–vis absorption (a) and emission (b) spectra of complexes **Ir1**-**Ir4** in CH_2Cl_2 solution at room temperature.

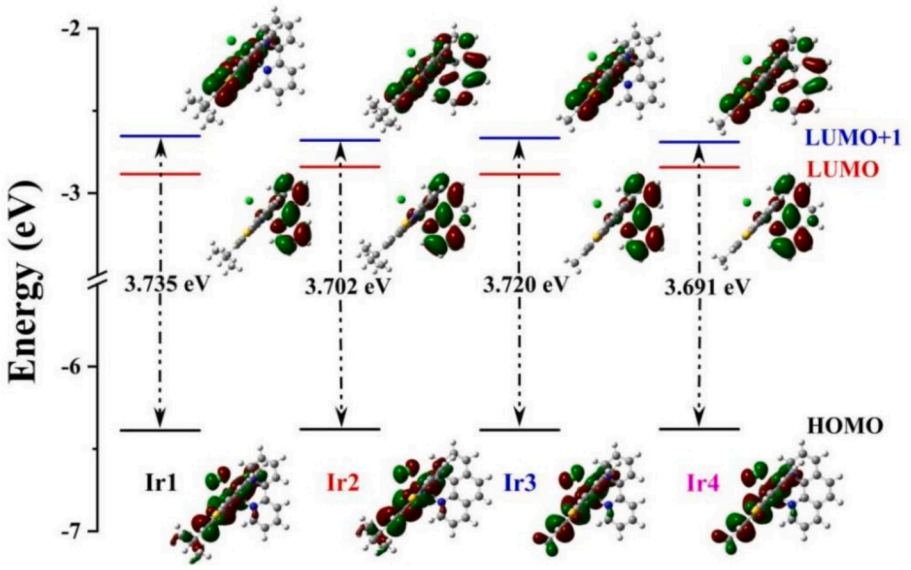

Fig. 3. Electronic levels and surface distributions of selected frontier molecular orbitals involved in crucial electronic excitations of complexes **Ir1**-**Ir4**.

the range 0.48 to 1.15 μs (Table S1). The quantum yields of **Ir1**-**Ir2** are less than the others, reflecting in the higher k_{nr} and lower k_r values, as a consequence of the relatively strong vibrational quenching effect caused by the presence of the two *t*-Bu groups on the NˆCˆN ligand.

Due to the overall photophysical properties of **Ir1**-**Ir4**, their cellular accumulation, uptake and distribution could be more easily monitored by laser scanning confocal microscopy. Thereby, these complexes were taken forward for anticancer testing.

2.3. Detection of lipophilicity and cytotoxicity

Before proceeding with anticancer studies, the lipophilicity of iridium complexes **Ir1**-**Ir4** were first tested by the partition coefficient in *n*-octanol/water system ($logP_{o/w}$) that reflect their ability to pass through the cell membrane [60,61]. Using the classical shake-flask technique, the $logP_{o/w}$ values are determined as the order of **Ir2** (2.25) > **Ir1** (2.22) > **Ir4** (2.04) > **Ir3** (1.91). As can be seen, complex **Ir2** exhibits the highest lipophilicity that facilitates its uptake by cancer cells, suggesting the complex would possess good cytotoxicity activity.

The *in vitro* cytotoxicity of the four complexes against Hela, RKO, A549, MGC-803 cancer cells and BEAS-2B non-cancer cells were measured by using standard 3-(4,5-dimethylthiazol-2-yl)-2,5-diphenyltetrazolium bromide (MTT) assay and compared to cisplatin as reference (Table 1). It's remarkable that all investigated complexes are more active than cisplatin against four types of cancer cells, which suggests that benzothiazole unit in this system has favorable anticancer effect. Overall, their cytotoxicity follows the order: **Ir1**/**Ir2** > **Ir3**/**Ir4** > cisplatin, further confirming the necessity of high lipophilicity for improving anticancer activity [24]. In detail, complexes **Ir1**/**Ir2** (0.74–3.29 μM) offer the lower IC_{50} values than their counterparts **Ir3**/**Ir4** (1.14–5.06 μM), probably owing to the effect of the *t*-Bu groups. Furthermore, the IC_{50} values of **Ir2** against Hela, A549, MGC-803 cells are about 1.5-fold lower than those of **Ir1**, related with the nature of ancillary ligands. And the cytotoxic activity of **Ir2** on three above cancer cells are about 3.7, 9.0 and 9.0-fold higher than that of cisplatin, respectively. Considering the cisplatin-resistance and universality, the better candidate was finally assigned as A549 cells [62–64]. Besides, these benzothiazole-based iridium(III) complexes also exhibit high selectivity between cancer cells and non-cancer cells. In particular, **Ir2** reveals the largest selectivity index of 16.7 toward A549 and BEAS-2B cells, far surpassing that of cisplatin (SI:1.6). Thus, we selected **Ir2** and A549 cells for further investigation into the underlying mechanisms, since **Ir2** was not only more cytotoxic to A549 cells, but also less cytotoxic to normal cells.

Table 1
IC50 (μM) values of **Ir1**-**Ir4** and cisplatin toward different cell lines after 24 h of exposure.

Complex	Hela	RKO	A549	MGC-803	BEAS-2B	SI
Ir1	2.95 ± 0.08	0.94 ± 0.35	3.29 ± 0.26	1.13 ± 0.11	46.22 ± 0.81	14.0
Ir2	1.87 ± 0.25	1.98 ± 0.21	2.23 ± 0.08	0.74 ± 0.07	37.3 ± 1.24	16.7
Ir3	4.08 ± 0.18	2.9 ± 0.07	3.77 ± 0.52	1.9 ± 0.17	41.85 ± 0.44	11.1
Ir4	1.14 ± 0.08	5.06 ± 0.92	3.89 ± 0.20	1.7 ± 0.14	39.5 ± 0.85	10.2
Cisplatin	6.92 ± 0.33	9.90 ± 0.28	20.01 ± 1.96	6.70 ± 0.80	32.01 ± 0.63	1.6

Selectivity index (SI): IC_{50} ratio of BEAS-2B normal cells to A549 cancer cells.

2.4. Solution stability studies

In order to study the solution stability of complexes **Ir1**-**Ir4**, the ^1H NMR spectra in DMSO solution were recorded at different time intervals (5 min and 24 h) (Figs. S1-S4). There are no significant changes in these spectral patterns, suggesting that the metal−ligand bonds in complexes remain intact that support their potential as anticancer drug candidates. To further evaluate the feasibility for therapeutic application, the stability of representative complex **Ir2** was conducted using emission spectra in PBS:DMSO (99:1) solution at room temperature at different PH values (3−10) and times (0–180 min), respectively (Fig. S5). As shown, the luminescence intensity was almost unchanged, indicating that **Ir2** would have good biological stability under acidic/alkaline and normal cell conditions.

2.5. Cellular uptake mechanism and cellular localization

Because the cellular uptake mechanism is an important factor when evaluating **Ir2** as an antitumor drug, to ascertain this, four sequent of experiments were designed utilizing laser confocal microscopy based on the inherent luminescence property of the iridium(III) complex. A549 tumor cells were firstly incubated with **Ir2** at the normal temperature of the human body (37 °C) and a low temperature (4 °C), and then co-

cultured with carbonyl cyanide *m*-chlorophenylhydrazone (CCCP, metabolic inhibitor) and chloroquine (endocytic inhibitor), respectively. Fig. 4a shows that the cellular uptake are apparently suppressed when at 4 °C or CCCP pretreated, while that with chloroquine treatment remains almost unchanged, indicating an energy-dependent cellular uptake mechanism and not an endocytosis pathway.

To further explore the target location of **Ir2** in subcellular organelles, the status of mitochondria and lysosome in **Ir2**-treated A549 cells were investigated using Mito Tracker Deep Red (MTDR, mitochondrial red fluorescent dye) and Lysol Tracker Deep Red (LTDR, lysosomal red fluorescent dye). As shown in Fig. 4b, green and red fluorescence originate from **Ir2** and mitochondrial/lysosomal dye, respectively. The merge of the green and red fluorescence displays that **Ir2** mainly accumulates in the mitochondria and slightly distributes in the lysosome with a Pearson co-localization coefficient (PCC) of 0.89 and lower 0.41, respectively. These results demonstrate that **Ir2** could specially map to mitochondria of A549 cells.

2.6. Apoptosis assay

Apoptosis has been described as a "suicide" program in various cells, which is an orderly death regulated by genes [24]. It has been reported that some transition metal complexes based on Pt(II), Ru(II), Os(II), and Ir(III) can cause apoptosis and show anticancer activity [65,66]. Thus, the ability of **Ir2** to induce apoptosis in A549 cells double-stained with Annexin V-FITC/propidium iodide (PI) was detected by flow cytometry. When the concentrations of **Ir2** are 0.5, 1.0 and 2.0 × IC_{50}, the percentages of early and late apoptotic cells increase in a concentration-dependent manner (Fig. 5a), demonstrating **Ir2** could induce apoptosis of A549 cells to achieve the anticancer effect.

2.7. Cellular cycle arrest

The effect of **Ir2** on cell cycle progression was also investigated using flow cytometric analysis (Fig. 5b). As shown, **Ir2** could effectively block the A549 cell cycle in G0/G1 phase when compared with the control. At a gradient concentration (0.5–2.0 × IC_{50}), the percentage of cells in G0/G1 phase increases, accompanied by a corresponding reduction in the S and G2/M phases. The concentration-dependent results suggest that **Ir2** could induce G0/G1 phase cell cycle arrest and further cause a gradual initiation of apoptosis in A549 cells.

2.8. Western blotting assay

To understand the mechanism of **Ir2**-induced antitumor effects, Western blot analysis was utilized to identify mitochondrial apoptosis pathways in A549 cells by detecting the level of Caspase-3 and Bcl-2 family proteins (Fig. 6). The activation of Caspase-3 represents an early event of apoptosis, which cleaves key structural proteins and ultimately leads to apoptotic cell death [67,68]. Bcl-2 is in the outer membrane of mitochondria, whose over expression can inhibit apoptosis. Bax is a core member of the Bcl-2 family proteins, which can form a heterodimer with Bcl-2 to make apoptosis more likely to occur [69]. In comparison to the control, the expression levels of Caspase-3 and pro-apoptotic protein Bax are increased while the anti-apoptosis protein Bcl-2 are decreased. This confirms that **Ir2** could promote apoptosis of A549 cells through the classical mitochondrial pathway, proving the above co-localization experiment in the meantime.

2.9. Evaluation of reactive oxygen species (ROS) generation

In general, the overproduction of ROS induced by transition metal complexes could cause mitochondria mediated dysfunction and then lead to apoptosis [70,71]. In order to investigate the efficacy of **Ir2** inducing ROS production in A549 cells, 2′,7′-dichlorofluorescein diacetate (DCFH-DA) probe was used to observe changes of intracellular ROS level using confocal imaging and flow cytometry. DCFH-DA can be hydrolyzed by esterase to non-fluorescent DCFH, and then be oxidized to generate highly fluorescent DCF by cellular ROS [72]. From Fig. 7a, it can be seen that the fluorescence in control cells is weak, whereas the fluorescence intensity in cells treated with **Ir2** gradually increase in a concentration-dependent manner. Next, the ROS levels were further established by flow cytometry (Fig. 7b). The ROS levels increased by 1.3 times when the concentration of **Ir2** was from 0.5 × IC_{50} to 2.0 × IC_{50}. Together, these results suggest that **Ir2** could effectively induce intracellular ROS production and promote apoptosis.

2.10. Mitochondrial membrane potential (MMP) changes

Most transition metal complexes can induce the loss of MMP and

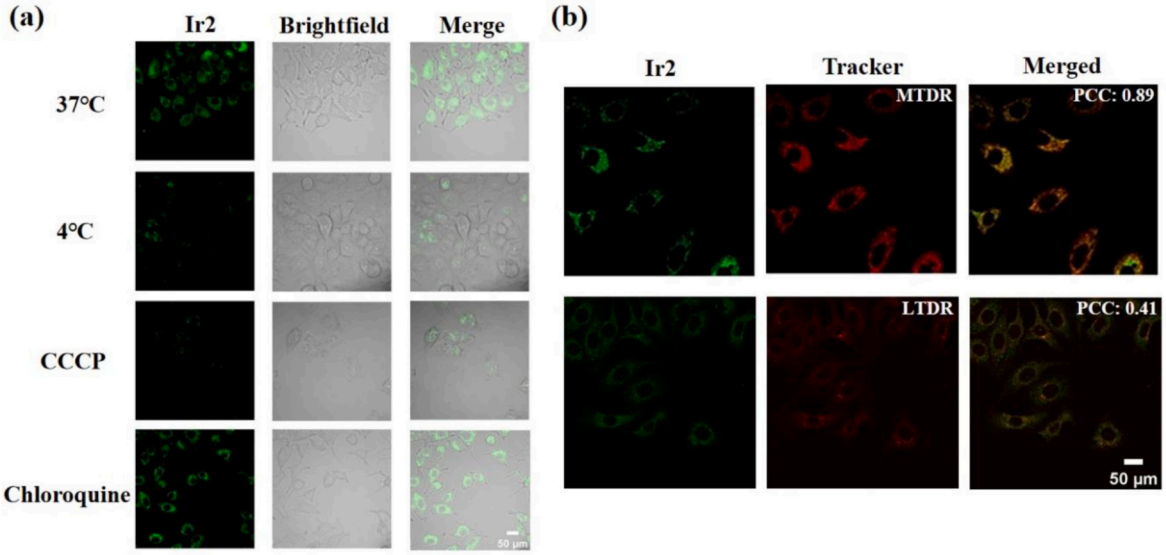

Fig. 4. (a) Confocal images of A549 cells treated with **Ir2** at 37 °C or 4 °C, and then incubated with CCCP or chloroquine at 37 °C. (b) Colocalization images of **Ir2** with MTDR and LTDR in A549 cells. **Ir2**: λ_{ex} = 445 nm, λ_{em} = 520 ± 30 nm; MTDR: λ_{ex} = 561 nm, λ_{em} = 600 ± 30 nm; LTDR: λ_{ex} = 594 nm, λ_{em} = 630 ± 30 nm. Scale bar: 50 μm.

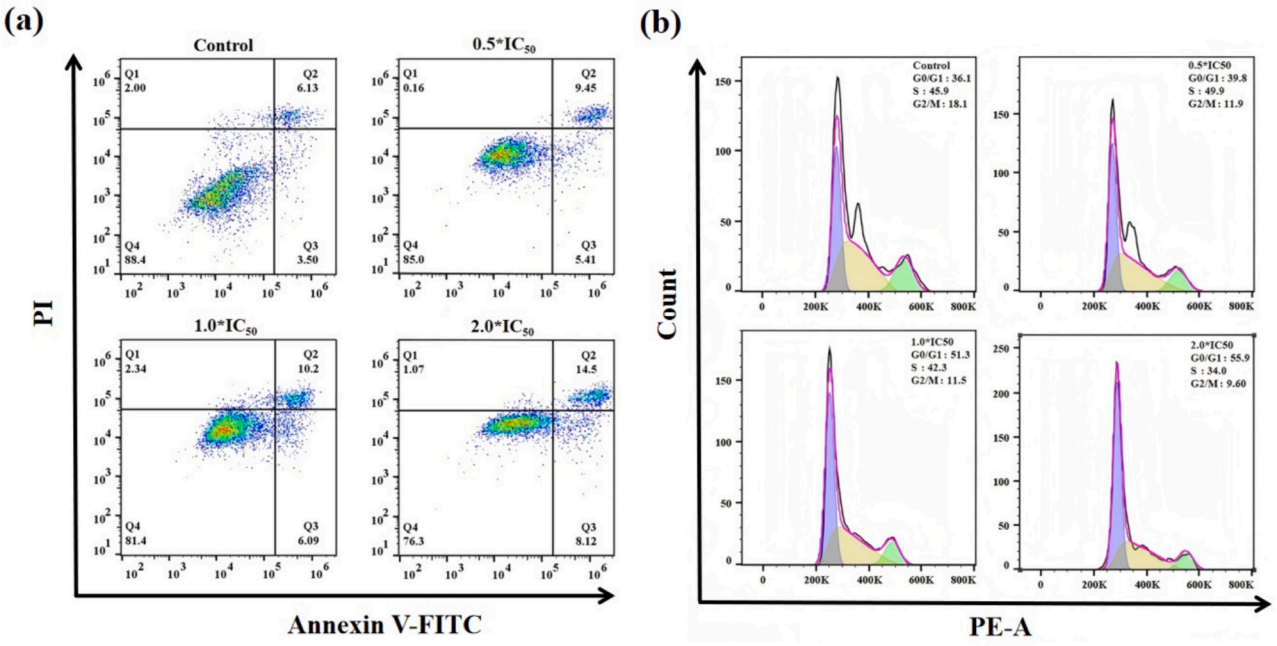

Fig. 5. Apoptosis assay (a) and cell cycle analysis (b) of A549 cells treated with **Ir2** at a gradient IC_{50} concentration.

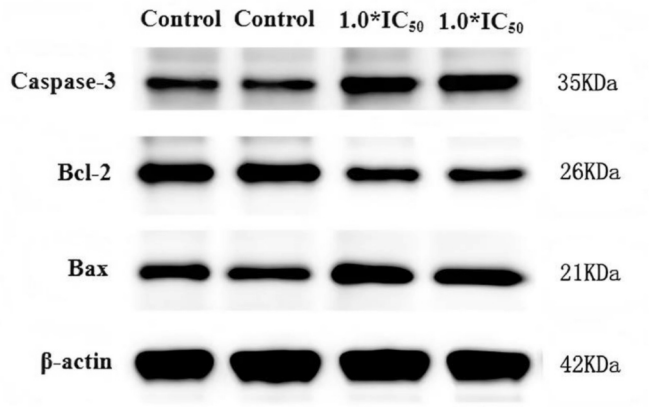

Fig. 6. Western blot analysis of Caspase-3 and Bcl-2 family proteins after treatment of **Ir2** at 1.0 × IC_{50} concentration.

activate mitochondria-related apoptotic pathways [71,73]. Therefore, the changes of MMP in **Ir2**-treated cells were detected using the 5,5′,6,6′-tetrachloro-1,1′,3,3′-tetraethylbenzimidazolylcarbocyanine iodide (JC-1) fluorescent probe. In high mitochondrial membrane potential, JC-1 aggregates emit red fluorescence; in contrast, when the mitochondria are damaged and the membrane potential decreases, JC-1 monomers emit green fluorescence [74]. As seen in Fig. 8a, the negative control group emits strong red fluorescence, while the cells treated with **Ir2** emit green fluorescence concentration-dependently, especially the positive control group of CCCP emits strong green fluorescence. Flow cytometry analysis was also performed to quantify MMP in **Ir2**-treated cells and Fig. 8b illustrates the experiment results. Compared with the negative control (14.5 %), the percentage of mitochondrial membrane depolarized cells increases by 31.7 % at 2.0 × IC_{50}, and exhibits a dose-dependent trend. Altogether, the above results confirms **Ir2** could induce mitochondrial dysfunction in A549 cells and eventually lead to apoptosis.

2.11. *In vivo antitumor and safety analysis*

After elucidating the apoptosis-inducing mechanism of **Ir2** *in vitro*, its antitumor efficacy and biosafety *in vivo* were evaluated. The BALB/c nude mice were subcutaneously implanted with A549 cells to obtain xenograft tumors, and then injected intratumorally with saline/DMSO, cisplatin, and **Ir2**, respectively. The body weight and tumor volume of the mice in each group were recorded every two days throughout the entire treatment period. After 14 days of treatment, the tumors were excised for photographing and weighing. From Figs. 10a-10b, tumors treated in **Ir2** group are significantly diminished compared with those in the cisplatin group and control group. Concretely, the tumor weights of the three groups are 1.54 ± 0.38 g, 3.78 ± 0.34 g and 6.63 ± 0.57 g, respectively (Fig. 9c and Table S6). Besides, the growth rates of the tumor volume and final volume in **Ir2** group are obviously smaller than those of the other two groups (Fig. 9 and Table S7). Furthermore, the tumor inhibition rates of the cisplatin and **Ir2** groups are 27.25 % and 71.60 %, respectively, confirming that **Ir2** has excellent antitumor efficacy. During the follow-up period, the mean body weight of mice in three test groups remained within the normal range (Fig. 9e and Table S8), indicating **Ir2** has low systemic toxicity and high biocompatibility [75,76].

At the end of treatment, the pathological tissues of the tumors in each group were examined by hematoxylin-eosin (H&E) staining (Fig. 10a). It is clearly that **Ir2**-treated group decreases more tumor cell density than the control and cisplatin groups, suggesting that **Ir2** could induce a serious death of tumor cells. In addition, the cells of major organs (heart, liver, spleen, lung and kidney) in the control and **Ir2** groups were also stained by H&E (Fig. 10b) and no abnormalities or signs of inflammation were observed in any organs for the **Ir2** group. Taken together, the above experimental results imply that **Ir2** has high antitumor efficacy and good *vivo* safety, thus could be a tumor-targeting candidate drug for A549 cancer.

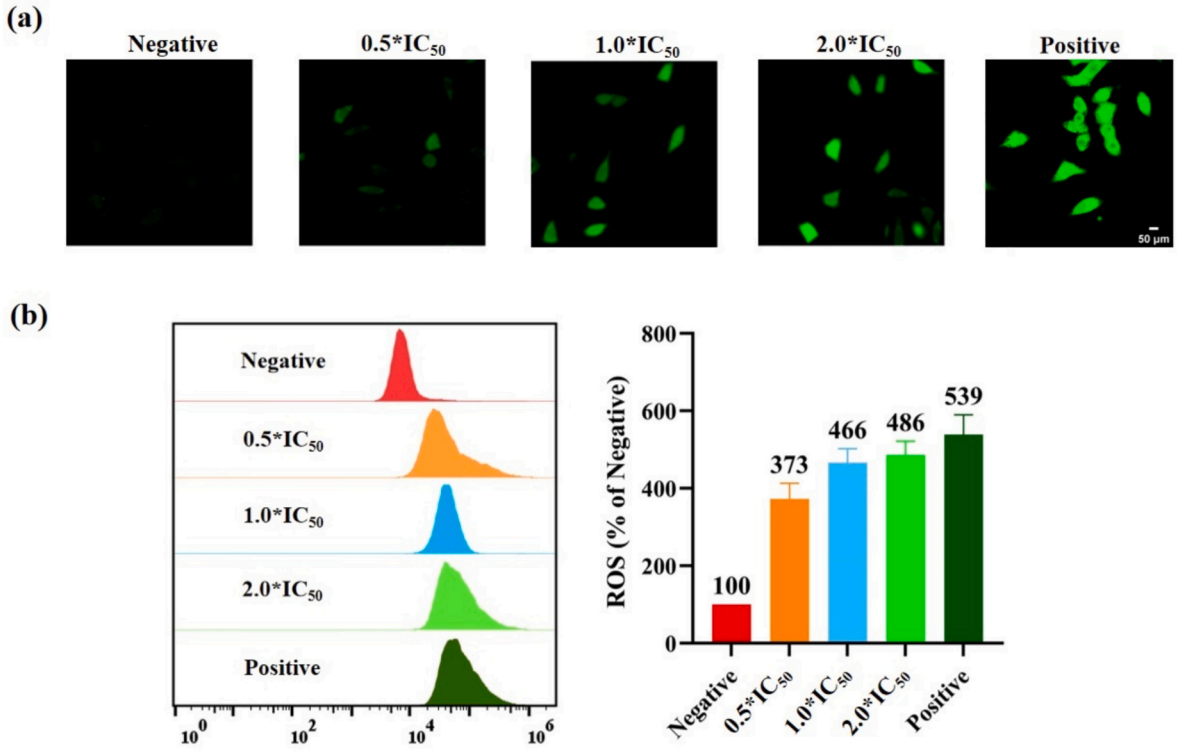

Fig. 7. (a) Intracellular ROS production in A549 cells treated with **Ir2** at a gradient IC_{50} concentration and stained with DCFH-DA. DCF: $\lambda_{ex} = 488$ nm, $\lambda_{em} = 540 \pm 20$ nm. Scale bar: 50 μm. (b) Intracellular ROS levels in A549 cells after treatment of **Ir2** at a gradient IC_{50} concentration; Histograms of relative ROS levels, and the data are the mean of three replicate experiments ± SD.

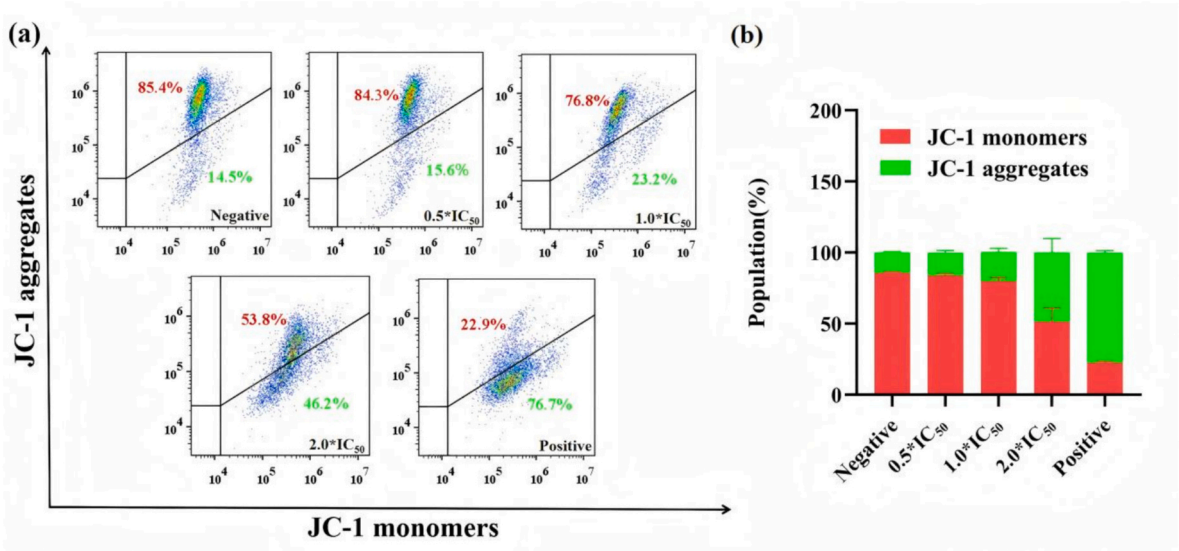

Fig. 8. (a) Changes in the MMP of A549 cells treated with **Ir2** at a gradient IC_{50} concentration and stained with JC-1. (b) Histogram of relative MMP changes, and the data are the mean of three replicate experiments ± SD.

3. Experimental section

3.1. Synthesis of ligands

3.1.1. 2,2′-(5-(tert-butyl)-1,3-phenylene)bis(benzo[d]thiazole) (L_1)

A mixture of 5-*tert*-butylisophthalic acid (1.00 g, 4.50 mmol), 2-aminothiophenol (1.24 g, 9.90 mmol), triphenyl phosphite (2.79 g, 9.00 mmol) and tetrabutylammonium bromide (2.9 g, 9.00 mmol) was heated to 120 °C and stirred for 2 h in a nitrogen atmosphere. After the reaction mixture was cooled to room temperature, methanol (20 ml) was added to precipitate a white solid and collected to give the desired product $\mathbf{L_1}$ as a white solid (1.30 g, 72.2 %). ^{1}H NMR (400 MHz, $CDCl_3$) δ 8.55 (t, J = 1.6 Hz, 1H), 8.28 (d, J = 1.6 Hz, 2H), 8.13 (d, J = 8.1 Hz, 2H), 7.95 (d, J = 8.0 Hz, 2H), 7.55–7.51 (m, 2H), 7.44–7.40 (m, 2H), 1.50 (s, 9H). HRMS: m/z 423.0956 $[M + Na]^+$ (calcd 423.1068).

3.1.2. 2,2′-(5-(methyl)-1,3-phenylene)bis(benzo[d]thiazole) (L_2)

$\mathbf{L_2}$ was synthesized according to the method described in $\mathbf{L_1}$ (white

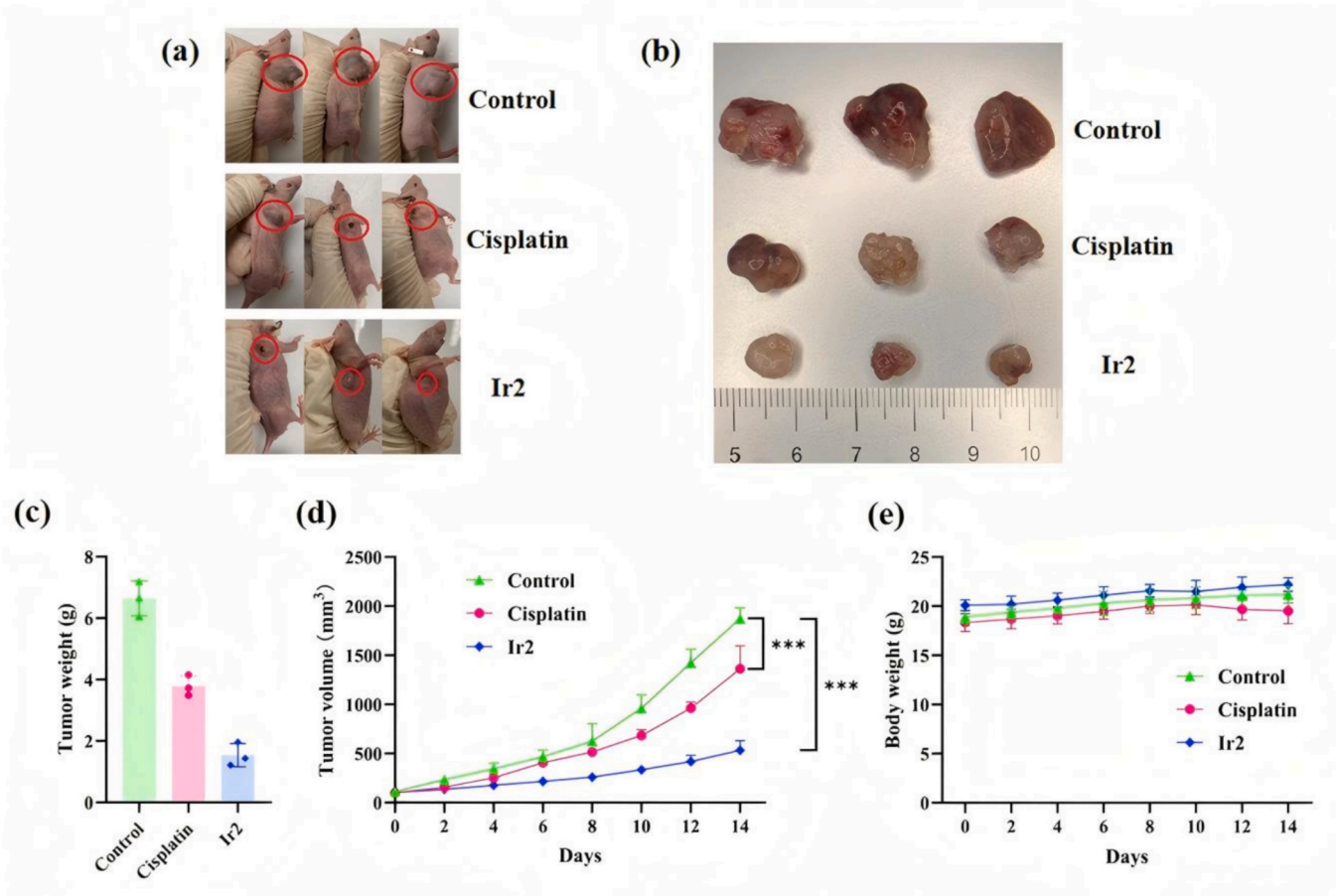

Fig. 9. Photographs of tumor *in vivo* (a), tumor sizes (b) and tumor weight (c) in control and cisplatin/**Ir2**-treated groups (3.0 mg/kg) at the end of treatment. The tumor volume (d) and changes in body weight (e) of each group throughout the follow-up period. The data are the mean of three replicate experiments ± SD.

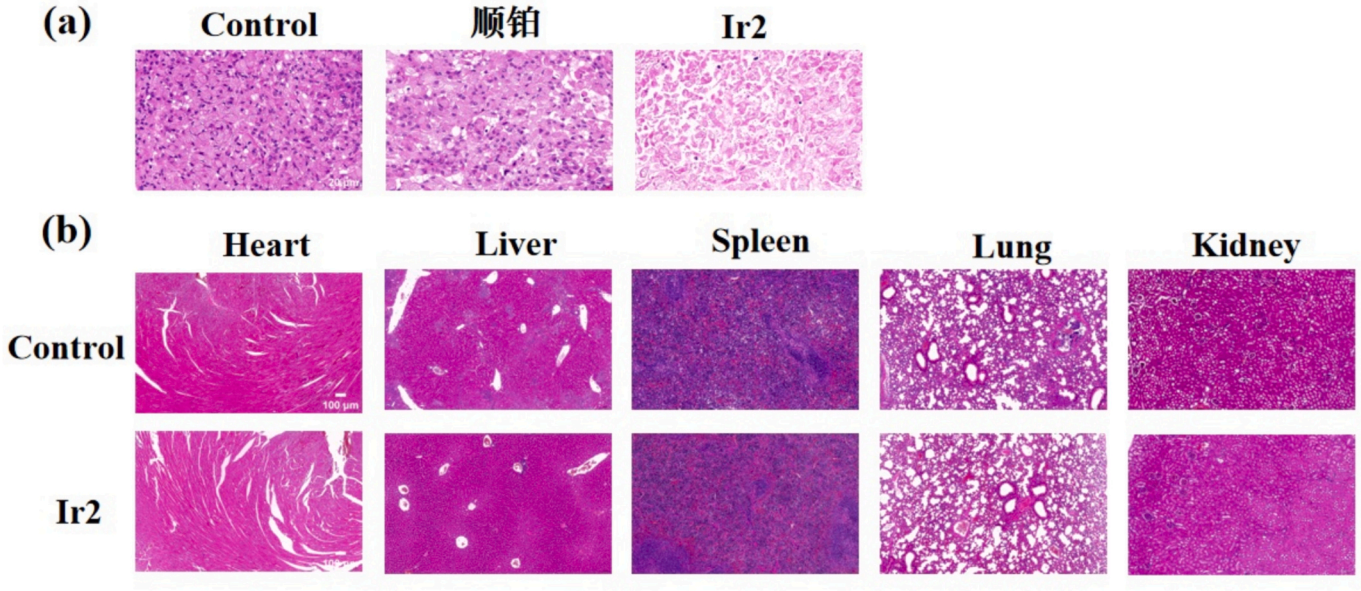

Fig. 10. H&E staining of tumor tissues in three groups (a, scale bar: 20 μm) and major organs of mice in two groups (b, scale bar: 100 μm) at the end of treatment.

solid, yield: 76.9 %). ^{1}H NMR (400 MHz, $CDCl_3$) δ 8.56 (d, J = 0.4 Hz, 1H), 8.12 (dd, J = 8.1, 0.4 Hz, 2H), 8.07 (dd, J = 1.6, 0.7 Hz, 2H), 7.95 (dd, J = 8.0, 0.6 Hz, 2H), 7.55–7.51 (m, 2H), 7.44–7.40 (m, 2H), 2.56 (s, 3H). HRMS: m/z 381.0487 $[M + Na]^+$ (calcd 381.0598).

3.2. Synthesis of Ir(III) complexes

$IrCl_3 \cdot 3H_2O$ (1.0 eq.) and $\mathbf{L_1}$/$\mathbf{L_2}$ (1.0 eq.) were dissolved in a mixture of 2-ethoxyethanol and water (v:v = 2:1), and then heated at 120 °C for

8 h under nitrogen atmosphere. After cooling to room temperature, the iridium dimer was filtered and dried, which was used in next step without further purification. A mixture of the iridium dimer, 2,2′-bipyridine/1,10-phenanthroline and silver trifluoromethyl sulfonate were dissolved in toluene and heated at 110 °C for 12 h under nitrogen atmosphere. After the reaction was completed, the solvent was removed *in vacuo*, then dichloromethane and water was added. The separated organic phase was washed with brine, dried over Na_2SO_4, filtered, and concentrated *in vacuo*. The residue was purified by flash column chromatography (DCM: MeOH = 100: 1–20: 1) to give complexes **Ir1**-**Ir4**.

Ir1 (yellow-green solid, yield: 25.4 %). ^{1}H NMR (400 MHz, $CDCl_3$) δ 10.43 (d, J = 4.7 Hz, 1H), 9.36 (d, J = 8.5 Hz, 1H), 8.95 (d, J = 7.8 Hz, 1H), 8.77 (t, J = 8.0 Hz, 1H), 8.32–8.22 (m, 1H), 8.08 (s, 2H), 7.91 (t, J = 7.9 Hz, 1H), 7.85 (d, J = 7.9 Hz, 2H), 7.41 (t, J = 7.4 Hz, 2H), 7.23–7.17 (m, 2H), 7.18–7.06 (m, 2H), 6.23 (d, J = 8.5 Hz, 2H), 1.62 (s, 9H). ^{13}C NMR (101 MHz, DMSO-d_6) δ 179.75, 169.05, 157.42, 156.31, 153.97, 150.27, 148.85, 148.25, 141.92, 139.86, 137.72, 131.24, 129.54, 129.06, 128.34, 126.21, 125.56, 125.16, 124.86, 116.84, 31.54. HRMS: m/z 783.0972 (calcd 783.0995). Anal. Calcd for $C_{35}H_{27}ClF_3IrN_4O_3S_3$: C, 45.08; H, 2.92; N, 6.01; found: C, 45.10; H, 2.89; N, 6.04.

Ir2 (yellow-green solid, yield: 20.6 %). ^{1}H NMR (400 MHz, $CDCl_3$) δ 10.72 (d, J = 5.0 Hz, 1H), 9.27 (d, J = 8.3 Hz, 1H), 8.66 (dd, J = 8.3, 5.0 Hz, 1H), 8.54 (d, J = 7.0 Hz, 1H), 8.46 (d, J = 8.9 Hz, 1H), 8.24 (d, J = 9.0 Hz, 1H), 8.14 (s, 2H), 7.81–7.77 (m, 2H), 7.69 (dd, J = 8.2, 5.5 Hz, 1H), 7.60 (d, J = 4.3 Hz, 1H), 7.32–7.26 (m, 2H), 7.00 (t, J = 7.9 Hz, 2H), 6.02 (d, J = 8.4 Hz, 2H), 1.65 (s, 9H). ^{13}C NMR (101 MHz, DMSO-d_6) δ 179.72, 168.21, 154.89, 151.48, 148.93, 148.32, 148.06, 146.71, 140.81, 139.21, 137.88, 131.17, 130.65, 128.52, 128.49, 128.12, 127.83, 127.13, 126.07, 125.16, 124.72, 116.69, 31.57. HRMS: m/z 807.0969 (calcd 807.0995). Anal. Calcd for $C_{37}H_{27}ClF_3IrN_4O_3S_3$: C, 46.46; H, 2.85; N, 5.86; found: C, 46.48; H, 2.88; N, 5.87.

Ir3 (yellow-green solid, yield: 23.4 %). ^{1}H NMR (400 MHz, $CDCl_3$) δ 10.42 (d, J = 4.4 Hz, 1H), 9.35 (d, J = 8.2 Hz, 1H), 8.93 (d, J = 8.2 Hz, 1H), 8.77 (t, J = 8.0 Hz, 1H), 8.31–8.20 (m, 1H), 7.95–7.87 (m, 3H), 7.84 (d, J = 8.0 Hz, 2H), 7.40 (t, J = 7.3 Hz, 2H), 7.20 (t, J = 7.9 Hz, 3H), 7.16–7.04 (m, 1H), 6.22 (d, J = 8.5 Hz, 2H), 2.76 (s, 2H). ^{13}C NMR (101 MHz, DMSO-d_6) δ 179.45, 168.92, 157.47, 156.34, 153.96, 150.29, 148.90, 141.98, 139.93, 137.85, 134.69, 131.25, 129.58, 129.04, 128.51, 128.41, 126.28, 125.63, 124.94, 116.87, 31.59. HRMS: m/z 741.0505 (calcd 741.0525). Anal. Calcd for $C_{32}H_{21}ClF_3IrN_4O_3S_3$: C, 43.17; H, 2.38; N, 6.29; found: C, 43.20; H, 2.42; N, 6.30.

Ir4 (yellow-green solid, yield: 28.4 %). ^{1}H NMR (400 MHz, $CDCl_3$) δ 10.71 (d, J = 5.0 Hz, 1H), 9.25 (d, J = 8.3 Hz, 1H), 8.66 (dd, J = 8.2, 5.0 Hz, 1H), 8.51 (d, J = 8.0 Hz, 1H), 8.45 (d, J = 8.9 Hz, 1H), 8.23 (d, J = 9.0 Hz, 1H), 7.97 (s, 2H), 7.79 (d, J = 8.0 Hz, 2H), 7.72–7.60 (m, 2H), 7.30 (d, J = 7.2 Hz, 2H), 6.99 (t, J = 8.4 Hz, 2H), 6.01 (d, J = 8.3 Hz, 2H), 2.79 (s, 3H). ^{13}C NMR (101 MHz, DMSO-d_6) δ 179.42, 168.10, 154.52, 151.63, 148.97, 148.14, 147.00, 142.45, 140.98, 139.26, 138.02, 134.77, 131.17, 130.68, 128.53, 128.21, 127.92, 127.10, 126.15, 124.80, 116.73, 31.59. HRMS: m/z 765.0504 (calcd 765.0525). Anal. Calcd for $C_{34}H_{21}ClF_3IrN_4O_3S_3$: C, 44.66; H, 2.31; N, 6.13; found: C, 44.62; H, 2.35; N, 6.16.

4. Conclusions

In this study, a novel set of benzothiazole-based tridentate iridium (III) complexes, **Ir1**-**Ir4**, have been synthesized and characterized. Their photophysical properties and antitumor activities have been investigated. All complexes exhibit relatively higher cytotoxicity toward selected four cancer cells compared to cisplatin and good selectivity between cancer cells and non-cancer cells. Especially, complex **Ir2** with high lipophilicity has a excellent performance on A549 cells, thus its antitumor mechanism was further studied. Through energy-dependent endocytosis, **Ir2** effectively targeted the mitochondria, and then induced apoptosis of A549 cells following classical mitochondrial pathway, such as increasing intracellular ROS levels, decreasing mitochondrial membrane potential and regulating the expression of Caspase-3 and Bcl-2 family proteins. Another study shows that **Ir2** could induce cell cycle arrest in the G0/G1 phase, inhibit the growth of cancer cells and eventually trigger apoptosis. Most notably, **Ir2** displays a higher anticancer efficacy compared to cisplatin in a mouse tumor model. Overall, our results pave a way for designing new tridentate-type iridium(III) complexes as effective drugs for cancer treatment.

CRediT authorship contribution statement

Qin Zhou: Writing – original draft, Validation, Investigation, Formal analysis, Data curation. **Xiao-Bin Zhang:** Validation, Investigation, Formal analysis, Data curation. **An-Li Liu:** Investigation, Formal analysis. **Zhi-Gang Niu:** Writing – review & editing, Supervision, Project administration, Funding acquisition, Conceptualization. **Gao-Nan Li:** Writing – review & editing, Supervision, Project administration, Funding acquisition, Conceptualization. **Fa-Biao Yu:** Supervision, Software, Resources, Funding acquisition, Data curation.

Declaration of competing interest

The authors declare that they have no known competing financial interests or personal relationships that could have appeared to influence the work reported in this paper.

Acknowledgments

This work was supported by the National Natural Science Foundation of China (22061016, 22261016, 22264013), the Natural Science Foundation of Hainan Province (225RC746, 823MS042) and the Grants for the Innovation Center of Academician Sun Shigang's Team in Hainan Province.

Appendix A. Supplementary data

Supplementary data to this article can be found online at https://doi.org/10.1016/j.bioorg.2025.108507.

Data availability

Data will be made available on request.

References

[1] U. Das, B. Kar, S. Pete, P. Paira, Ru(II), Ir(III), re(I) and Rh(III) based complexes as next generation anticancer metallopharmaceuticals, Dalton Trans. 50 (2021) 11259–11290, https://doi.org/10.1039/d1dt01326b.
[2] W.Y. Zhang, Y.J. Wang, F. Du, M. He, Y.Y. Gu, L. Bai, L.L. Yang, Y.J. Liu, Evaluation of anticancer effect in vitro and in vivo of iridium(III) complexes on gastric carcinoma SGC-7901 cells, Eur. J. Med. Chem. 178 (2019) 401–416, https://doi.org/10.1016/j.ejmech.2019.06.003.
[3] P. Jia, R. Ouyang, P. Cao, X. Tong, X. Zhou, T. Lei, Y. Zhao, N. Guo, H. Chang, Y. Miao, S. Zhou, Review: recent advances and future development of metal complexes as anticancer agents, J. Coord. Chem. 70 (2017) 2175–2201, https://doi.org/10.1080/00958972.2017.1349313.
[4] E. Ortega, G. Vigueras, F.J. Ballester, J. Ruiz, Targeting translation: a promising strategy for anticancer metallodrugs, Coord. Chem. Rev. 446 (2021) 214129, https://doi.org/10.1016/j.ccr.2021.214129.
[5] J. Masternak, A. Gilewska, B. Barszcz, I. Łakomska, K. Kazimierczuk, J. Sitkowski, J. Wietrzyk, A. Kamecka, M. Milczarek, Ruthenium(II) and iridium(III) complexes as tested materials for new anticancer agents, Materials 13 (2020) 3491, https://doi.org/10.3390/ma13163491.
[6] C.C. Konkankit, S.C. Marker, K.M. Knopf, J.J. Wilson, Anticancer activity of complexes of the third row transition metals, rhenium, osmium, and iridium, Dalton Trans. 47 (2018) 9934, https://doi.org/10.1039/c8dt01858h.
[7] C. Zhang, C. Xu, X. Gao, Q. Yao, Platinum-based drugs for cancer therapy and anti-tumor strategies, Theranostics 12 (2022) 2115–2132, https://doi.org/10.7150/thno.69424.
[8] M.N.D. Stojanović, A.A. Franich, M.M. Jurišević, N.M. Gajović, N.N. Arsenijević, I. P. Jovanović, B.S. Stojanović, S.J. Mitrović, J. Kljun, S. Rajković, M.D. Živković, Platinum(II) complexes with malonic acids: synthesis, characterization, in vitro

and in vivo antitumor activity and interactions with biomolecules, J. Inorg. Biochem. 231 (2022) 111773, https://doi.org/10.1016/j.jinorgbio.2022.111773.
[9] R. Ali, M. Aouida, A.A. Sulaiman, S. Madhusudan, D. Ramotar, Can cisplatin therapy be improved? Pathways that can be targeted, Int. J. Mol. Sci. 23 (2022) 7241, https://doi.org/10.3390/ijms23137241.
[10] M.T. Wlodarczyk, S.A. Dragulska, O. Camacho-Vanegas, P.R. Dottino, A. A. Jarzęcki, J.A. Martignetti, A.J. Mieszawska, Platinum(II) complex-nuclear localization sequence peptide hybrid for overcoming platinum resistance in cancer therapy, Acs Biomater-sci. Eng. 4 (2018) 463–467, https://doi.org/10.1021/acsbiomaterials.7b00921.
[11] Y.Y. Ling, W.J. Wang, L. Hao, X.W. Wu, J.H. Liang, H. Zhang, Z.W. Mao, C.P. Tan, Self-amplifying iridium(III) photosensitizer for ferroptosis mediated immunotherapy against transferrin receptor overexpressing cancer, Small 18 (2022) 2203659, https://doi.org/10.1002/smll.202203659.
[12] X. Su, W.J. Wang, Q. Cao, H. Zhang, B. Liu, Y. Ling, X. Zhou, Z.W. Mao, A carbonic anhydrase IX (CAIX)-anchored rhenium(I) photosensitizer evokes pyroptosis for enhanced anti-tumor immunity, Angew. Chem. Int. Ed. 61 (2022) e202115800, https://doi.org/10.1002/anie.202115800.
[13] X.X. Peng, H. Zhang, R. Zhang, Z.H. Li, Z.S. Yang, J. Zhang, S. Gao, J.L. Zhang, Gallium triggers ferroptosis through a synergistic mechanism, Angew. Chem. Int. Ed. 62 (2023) e202307838, https://doi.org/10.1002/anie.202307838.
[14] Z. Yang, S. Huang, Y. Liu, X. Chang, Y. Liang, X. Li, Z. Xu, S. Wang, Y. Lu, Y. Liu, W. Liu, Biotin-targeted au(I) radiosensitizer for cancer synergistic therapy by intervening with redox homeostasis and inducing ferroptosis, J. Med. Chem. 65 (2022) 8401–8415, https://doi.org/10.1021/acs.jmedchem.2c00300.
[15] Y. Lai, N. Lu, S. Luo, H. Wang, P. Zhang, A photoactivated sorafenib-ruthenium(II) prodrug for resistant hepatocellular carcinoma therapy through ferroptosis and purine metabolism disruption, J. Med. Chem. 65 (2022) 13041–13051, https://doi.org/10.1021/acs.jmedchem.2c00880.
[16] M. Hołota, J. Magiera, S. Michlewska, M. Kubczak, N. Sanz del Olmo, S. García-Gallego, P. Ortega, F.J. de la Mata, M. Ionov, M. Bryszewska, In vitro anticancer properties of copper metallodendrimers, Biomolecules 9 (2019) 155, https://doi.org/10.3390/biom9040155.
[17] K. Máliková, L. Masaryk, P. Štarha, Anticancer half-sandwich rhodium(III) complexes, Inorganics 9 (2021) 26, https://doi.org/10.3390/inorganics9040026.
[18] Q. Zhao, C. Huang, F. Li, Phosphorescent heavy-metal complexes for bioimaging, Chem. Soc. Rev. 40 (2011) 2508–2524, https://doi.org/10.1039/c0cs00114g.
[19] X. Zheng, H. Tang, C. Xie, J. Zhang, W. Wu, X. Jiang, Tracking cancer metastasis in vivo by using an iridium-based hypoxia-activated optical oxygen nanosensor, Angew. Chem. Int. Ed. 54 (2015) 8094–8099, https://doi.org/10.1002/anie.201503067.
[20] J. Hao, H. Liu, J. Wang, X. Wang, C. Huang, L. Liang, J. Chen, Y. Wang, Y. Liu, Iridium(III) complexes induce cervical carcinoma apoptosis via disturbing cellular redox homeostasis disorder and inhibiting PI3K/AKT/mTOR pathway, J. Inorg. Biochem. 235 (2022) 111946, https://doi.org/10.1016/j.jinorgbio.2022.111946.
[21] S. Kuang, L. Sun, X. Zhang, X. Liao, T.W. Rees, L. Zeng, Y. Chen, X. Zhang, L. Ji, H. Chao, A mitochondrion-localized two-photon photosensitizer generating carbon radicals against hypoxic tumors, Angew. Chem. Int. Ed. 59 (2020) 20697–20703, https://doi.org/10.1002/anie.202009888.
[22] A. Sharma, P. Sudhindra, N. Roy, P. Paira, Advances in novel iridium(III) based complexes for anticancer applications: a review, Inorg. Chim. Acta 513 (2020) 119925, https://doi.org/10.1016/j.ica.2020.119925.
[23] X. Liu, A. Lv, P. Zhang, J. Chang, R. Dong, M. Liu, J. Liu, X. Huang, X.A. Yuan, Z. Liu, The anticancer application of half-sandwich iridium(III) ferrocene-thiosemicarbazide Schiff base complexes, Dalton Trans. 53 (2024) 552–563, https://doi.org/10.1039/d3dt02879h.
[24] L. Wang, X. Liu, Y. Wu, X. He, X. Guo, W. Gao, L. Tan, X.A. Yuan, J. Liu, Z. Liu, In vitro and in vivo antitumor assay of mitochondrially targeted fluorescent half-sandwich iridium(III) pyridine complexes, Inorg. Chem. 62 (2023) 3395–3408, https://doi.org/10.1021/acs.inorgchem.2c03333.
[25] Z. Liu, P.J. Sadler, Organoiridium complexes: anticancer agents and catalysts, Acc. Chem. Res. 47 (2014) 1174–1185, https://doi.org/10.1021/ar400266c.
[26] A. Zamora, G. Vigueras, V. Rodríguez, M.D. Santana, J. Ruiz, Cyclometalated iridium(III) luminescent complexes in therapy and phototherapy, Coord. Chem. Rev. 360 (2018) 34–76, https://doi.org/10.1016/j.ccr.2018.01.010.
[27] D.L. Ma, D.S.H. Chan, C.H. Leung, Group 9 organometallic compounds for therapeutic and bioanalytical applications, Acc. Chem. Res. 47 (2014) 3614–3631, https://doi.org/10.1021/ar500310z.
[28] C. Caporale, M. Massi, Cyclometalated iridium(III) complexes for life scienc, Coord. Chem. Rev. 363 (2018) 71–91, https://doi.org/10.1016/j.ccr.2018.02.006.
[29] R.M. Lord, P.C. McGowan, Organometallic iridium arene compounds: the effects of C-donor ligands on anticancer activity, Chem. Lett. 48 (2019) 916–924, https://doi.org/10.1246/cl.190179.
[30] C. Yang, F. Mehmood, T.L. Lam, S.L.F. Chan, Y. Wu, C.S. Yeung, X. Guan, K. Li, C.Y. S. Chung, C.Y. Zhou, T. Zou, C.M. Che, Stable luminescent iridium(III) complexes with bis(N-heterocyclic carbene) ligands: photo-stability, excited state properties, visible-light-driven radical cyclization and CO_2 reduction, and cellular imaging, Chem. Sci. 7 (2016) 3123–3136, https://doi.org/10.1039/c5sc04458h.
[31] T.L. Lam, K.C. Tong, C. Yang, W.L. Kwong, X. Guan, M.D. Li, V.K.Y. Lo, S.L.F. Chan, D.L. Phillips, C.N. Lok, C.M. Che, Luminescent ruffled iridium(III) porphyrin complexes containing N-heterocyclic carbene ligands: structures, spectroscopies and potent antitumor activities under dark and light irradiation conditions, Chem. Sci. 10 (2019) 293–309, https://doi.org/10.1039/c8sc02920b.
[32] A. Bonfiglio, M. Mauro, Phosphorescent tris-bidentate Ir^{III} complexes with N-heterocyclic carbene scaffolds: structural diversity and optical properties, Eur. J. Inorg. Chem. 36 (2020) 3427–3442, https://doi.org/10.1002/ejic.202000509.
[33] L. Chen, H. Tang, W. Chen, J. Wang, S. Zhang, J. Gao, Y. Chen, X. Zhu, Z. Huang, J. Chen, Mitochondria-targeted cyclometalated iridium(III) complexes: dual induction of A549 cells apoptosis and autophagy, J. Inorg. Biochem. 249 (2023) 112397, https://doi.org/10.1016/j.jinorgbio.2023.112397.
[34] Q. Sun, Y. Wang, Q. Fu, A. Ouyang, S. Liu, Z. Wang, Z. Su, J. Song, Q. Zhang, P. Zhang, D. Lu, Sulfur-coordinated organoiridium(III) complexes exert breast anticancer activity via inhibition of Wnt/β-catenin signaling, Angew. Chem. Int. Ed. 133 (2021) 4891–4898, https://doi.org/10.1002/anie.202015009.
[35] Y.L. Zeng, L.Y. Liu, T.Z. Ma, Y. Liu, B. Liu, W. Liu, Q.H. Shen, C. Wu, Z.W. Mao, Iridium(III) photosensitizers induce simultaneous pyroptosis and ferroptosis for multi-network synergistic tumor immunotherapy, Angew. Chem. Int. Ed. 63 (2024) e202410803, https://doi.org/10.1002/anie.202410803.
[36] L. Wang, R. Guan, L. Xie, X. Liao, K. Xiong, T.W. Rees, Y. Chen, L. Ji, H. Chao, An er-targeting iridium(III) complex that induces immunogenic cell death in non-small-cell lung cancer, Angew. Chem. Int. Ed. 60 (2021) 4657–4665, https://doi.org/10.1002/anie.202013987.
[37] K. Peng, Y. Zheng, W. Xia, Z.W. Mao, Organometallic anti-tumor agents: targeting from biomolecules to dynamic bioprocesses, Chem. Soc. Rev. 52 (2023) 2790–2832, https://doi.org/10.1039/d2cs00757f.
[38] U. Sreelekha, U. Basu, P. Paira, Current context of designing phototheranostic cyclometalated iridium(III) complexes to open a new avenue in cancer therapy, ChemMedChem 20 (2025) e202400649, https://doi.org/10.1002/cmdc.202400649.
[39] Y. Hisamatsu, N. Suzuki, A.A. Masum, A. Shibuya, R. Abe, A. Sato, S. Tanuma, S. Aoki, Cationic amphiphilic tris-cyclometalated iridium(III) complexes induce cancer cell death via interaction with Ca^{2+}-calmodulin complex, Bioconjug. Chem. 28 (2016) 507–523, https://doi.org/10.1021/acs.bioconjchem.6b00627.
[40] V. Novohradsky, A. Marco, L. Markova, N. Cutillas, J. Ruiz, V. Brabec, Ir(III) compounds containing a terdentate ligand are potent inhibitors of proliferation and effective antimetastatic agents in aggressive triple-negative breast cancer cells, J. Med. Chem. 66 (2023) 9766–9783, https://doi.org/10.1021/acs.jmedchem.3c00586.
[41] H. Huang, S. Banerjee, K. Qiu, P. Zhang, O. Blacque, T. Malcomson, M.J. Paterson, G.J. Clarkson, M. Staniforth, V.G. Stavros, G. Gasser, H. Chao, P.J. Sadler, Targeted photoredox catalysis in cancer cells, Nat. Chem. 11 (2019) 1041–1048, https://doi.org/10.1038/s41557-019-0328-4.
[42] L. Wei, R. Kushwaha, A. Dao, Z. Fan, S. Banerjee, H. Huang, Axisymmetric bis-tridentate Ir(III) photoredox catalysts for anticancer phototherapy under hypoxia, Chem. Commun. 59 (2023) 3083–3086, https://doi.org/10.1039/d2cc06721h.
[43] B. Liu, S. Monro, Z. Li, M.A. Jabed, D. Ramirez, C.G. Cameron, K. Colón, J. Roque III, S. Kilina, J. Tian, S.A. McFarland, W. Sun, A new class of homoleptic and heteroleptic bis(terpyridine) iridium(III) complexes with strong photodynamic therapy effects, ACS Appl. Bio Mater. 2 (2019) 2964–2977, https://doi.org/10.1021/acsabm.9b00312.
[44] Z. Fan, Y. Rong, T. Sadhukhan, S. Liang, W. Li, Z. Yuan, Z. Zhu, S. Guo, S. Ji, J. Wang, R. Kushwaha, S. Banerjee, K. Raghavachari, H. Huang, Single-cell quantification of a highly biocompatible dinuclear iridium(III) complex for photocatalytic cancer therapy, Angew. Chem. Int. Ed. 134 (2022) e202202098, https://doi.org/10.1002/anie.202202098.
[45] B. Liu, S. Monro, L. Lystrom, C.G. Cameron, K. Colón, H. Yin, S. Kilina, S. A. McFarland, W. Sun, Photophysical and photobiological properties of dinuclear iridium(III) bis-tridentate complexes, Inorg. Chem. 57 (2018) 9859–9872, https://doi.org/10.1021/acs.inorgchem.8b00789.
[46] R. Guan, Y. Chen, L. Zeng, T.W. Rees, C. Jin, J. Huang, Z.S. Chen, L. Ji, H. Chao, Oncosis-inducing cyclometalated iridium(III) complexes, Chem. Sci. 9 (2018) 5183–5190, https://doi.org/10.1039/c8sc01142g.
[47] E. Brantley, V. Trapani, M.C. Alley, C.D. Hose, T.D. Bradshaw, M.F.G. Stevens, E. A. Sausville, S.F. Stinson, Fluorinated 2-(4-amino-3-methylphenyl) benzothiazoles induce CYP1A1 expression, become metabolized, and bind to macromolecules in sensitive human cancer cells, Drug Metab. Dispos. 32 (2004) 1392–1401, https://doi.org/10.1124/dmd.104.001057.
[48] T.D. Bradshaw, A.D. Westwell, The development of the antitumour benzothiazole prodrug, phortress, as a clinical candidate, Curr. Med. Chem. 11 (2004) 1009–1021, https://doi.org/10.2174/0929867043455530.
[49] H.K. Kim, M.K. Kang, K.H. Jung, S.H. Kang, Y.H. Kim, J.C. Jung, G.H. Lee, Y. Chang, T.J. Kim, Gadolinium complex of DO3A-benzothiazole aniline (BTA) conjugate as a theranostic agent, J. Med. Chem. 56 (2013) 8104–8111, https://doi.org/10.1021/jm401206t.
[50] M.V. Babak, M. Pfaffeneder-Kmen, S.M. Meier-Menches, M.S. Legina, S. Theiner, C. Licona, C. Orvain, M. Hejl, M. Hanif, M.A. Jakupec, B.K. Keppler, C. Gaiddon, C. G. Hartinger, Rollover cyclometalated bipyridine platinum complexes as potent anticancer agents: impact of the ancillary ligands on the mode of action, Inorg. Chem. 57 (2018) 2851–2864, https://doi.org/10.1021/acs.inorgchem.7b03210.
[51] J. Sanz-Villafruela, C. Bermejo-Casadesús, M. Martínez-Alonso, A. Moro, J.C. Lima, A. Massaguer, G. Espino, Towards efficient Ir(III) anticancer photodynamic therapy agents by extending π-conjugation on N^N ligands, Dalton Trans. 53 (2024) 11393–11409, https://doi.org/10.1039/D4DT00390J.
[52] R. Cao, J. Jia, X. Ma, M. Zhou, H. Fei, Membrane localized iridium(III) complex induces endoplasmic reticulum stress and mitochondria-mediated apoptosis in human cancer cells, J. Med. Chem. 56 (2013) 3636–3644, https://doi.org/10.1021/jm4001665.
[53] P. Brulatti, R.J. Gildea, J.A.K. Howard, V. Fattori, M. Cocchi, J.A.G. Williams, Luminescent iridium(III) complexes with N^C^N-coordinated terdentate ligands: dual tuning of the emission energy and application to organic light-emitting devices, Inorg. Chem. 51 (2012) 3813–3826, https://doi.org/10.1021/ic202756w.

[54] S. Takizawa, S. Katoh, A. Okazawa, N. Ikuta, S. Matsushima, F. Zeng, S. Murata, Triplet excited states modulated by push−pull substituents in monocyclometalated iridium(III) photosensitizers, Inorg. Chem. 60 (2021) 4891–4903, https://doi.org/10.1021/acs.inorgchem.0c03802.
[55] D.N. Chirdon, W.J. Transue, H.N. Kagalwala, A. Kaur, A.B. Maurer, T. Pintauer, S. Bernhard, [Ir(N^N^N)(C^N)L]$^{+}$: a new family of luminophores combining tunability and enhanced photostability, Inorg. Chem. 53 (2014) (2014) 1487–1499, https://doi.org/10.1021/ic402411g.
[56] X.B. Zhang, W.Y. Tong, M.S. Chen, J.L. Xie, Y.T. Wang, Z.R. Mo, S.X. Wu, Z.G. Niu, G.N. Li, Synthesis, photophysical properties, and DFT calculation of yellow-red phosphorescent iridium(III) complexes based on thiophen-pyrimidine/pyridine derivatives, J. Chin. Chem. Soc. 69 (2022) 2042–2048, https://doi.org/10.1002/jccs.202200370.
[57] Q. Zhao, S. Liu, M. Shi, C. Wang, M. Yu, L. Li, F. Li, T. Yi, C. Huang, Series of new cationic iridium(III) complexes with tunable emission wavelength and excited state properties: structures, theoretical calculations, and photophysical and electrochemical properties, Inorg. Chem. 45 (2006) 6152–6160, https://doi.org/10.1021/ic052034j.
[58] D.W. Li, Q. Zhou, X.C. Ma, B.W. Jia, J.Y. Huang, M.X. Mao, G.N. Li, Z.G. Niu, Cooperative structural modulation on main ligand and ancillary ligand in iridium (III) complexes to achieve high-performance OLEDs, J. Mol. Struct. 1332 (2025) 141648, https://doi.org/10.1016/j.molstruc.2025.141648.
[59] C. Wu, K.N. Tong, M. Zhang, M. Ng, S.W. Zhang, W. Cai, S. Jung, Y. Wu, C. Yang, M.C. Tang, G. Wei, Low efficiency roll-off blue phosphorescent OLEDs at high brightness based on [3+2+1] coordinated iridium(III) complexes, Adv. Optical Mater. 10 (2022) 2200356, https://doi.org/10.1002/adom.202200356.
[60] C.A. Puckett, J.K. Barton, Methods to explore cellular uptake of ruthenium complexes, J. Am. Chem. Soc. 129 (2007) 46–47, https://doi.org/10.1021/ja0677564.
[61] A. Ghezzi, M. Aceto, C. Cassino, E. Gabano, D. Osella, Uptake of antitumor platinum(II)-complexes by cancer cells, assayed by inductively coupled plasma mass spectrometry (ICP-MS), J. Inorg. Biochem. 98 (2004) 73–78, https://doi.org/10.1016/j.jinorgbio.2003.08.014.
[62] H. Hu, F. Zhang, Z. Sheng, S. Tian, G. Li, S. Tang, Y. Niu, J. Yang, Y. Liu, Synthesis and mitochondria-localized iridium(III)complexes induce celldeath through pyroptosis and ferroptosis pathways, Eur. J. Med. Chem. 268 (2024) 116295, https://doi.org/10.1016/j.ejmech.2024.116295.
[63] Y. Gu, H. Wen, L. Bai, Y. Zhou, H. Zhang, L. Tian, Y. Zhang, J. Hao, Y. Liu, Exploring anticancer efficiency of mitochondria-targeted cyclometalated iridium (III) complexes, J. Inorg. Biochem. 212 (2020) 111215, https://doi.org/10.1016/j.jinorgbio.2020.111215.
[64] H. Fu, S. Wang, Y. Gong, H. Dong, K. Lai, Z. Yang, C. Fan, Z. Liu, L. Guo, Triphenylphosphine-modified cyclometalated iridium(III) complexes as mitochondria-targeting anticancer agents with enhanced selectivity, Bioorg. Chem. 155 (2025) 108148, https://doi.org/10.1016/j.bioorg.2025.108148.
[65] I. Romero-Canelón, M. Mos, P.J. Sadler, Enhancement of selectivity of an organometallic anticancer agent by redox modulation, J. Med. Chem. 58 (2015) 7874–7880, https://doi.org/10.1021/acs.jmedchem.5b00655.
[66] R. Guan, L. Xie, L. Ji, H. Chao, Phosphorescent iridium(III) complexes for anticancer applications, Eur. J. Inorg. Chem. 2020 (2020) 3978–3986, https://doi.org/10.1002/ejic.202000754.
[67] Y. Shi, Caspase activation, inhibition, and reactivation: a mechanistic view, Protein Sci. 13 (2004) 1979–1987, https://doi.org/10.1110/ps.04789804.
[68] R.L. Panchangam, R.N. Rao, M.M. Balamurali, T.B. Hingamire, D. Shanmugam, V. Manickam, K. Chanda, Antitumor effects of Ir(III)-2H-indazole complexes for triple negative breast cancer, Inorg. Chem. 60 (2021) 17593–17607, https://doi.org/10.1021/acs.inorgchem.1c02193.
[69] Y. Wu, J. Liu, M. Shao, P. Zhang, S. Song, G. Yang, X. Liu, Z. Liu, Cyclometalated iridium(III) dithioformic acid complexes as mitochondria-targeted imaging and anticancer agents, J. Inorg. Biochem. 233 (2022) 111855, https://doi.org/10.1016/j.jinorgbio.2022.111855.
[70] S.S. Massoud, F.R. Louka, N.M.H. Salem, R.C. Fischer, A. Torvisco, F.A. Mautner, J. Vančo, J. Belza, Z. Dvořák, Z. Trávníček, Dinuclear doubly bridged phenoxido copper(II) complexes as efficient anticancer agents, Eur. J. Med. Chem. 246 (2023) 114992, https://doi.org/10.1016/j.ejmech.2022.114992.
[71] L.Q. Du, T.Y. Zhang, X.M. Huang, Y. Xu, M.X. Tan, Y. Huang, Y. Chen, Q.P. Qin, Synthesis and anticancer mechanisms of zinc(II)-8-hydroxyquinoline complexes with 1,10-phenanthroline ancillary ligands, Dalton Trans. 52 (2023) 4737–4751, https://doi.org/10.1039/d3dt00150d.
[72] Z.Y. Pan, B.F. Liang, Y.S. Zhi, D.H. Yao, C.Y. Li, H.Q. Wu, L. He, Near-infrared AIE-active phosphorescent iridium(III) complex for mitochondria-targeted photodynamic therapy, Dalton Trans. 52 (2023) 1291–1300, https://doi.org/10.1039/d2dt03861g.
[73] T. Chen, Y. Liu, W.J. Zheng, J. Liu, Y.S. Wong, Ruthenium polypyridyl complexes that induce mitochondria-mediated apoptosis in cancer cells, Inorg. Chem. 49 (2010) 6366–6368, https://doi.org/10.1021/ic100277w.
[74] Y. Gu, H. Wen, Y. Zhang, L. Bai, Y. Zhou, H. Zhang, L. Tian, J. Hao, Y. Liu, Studies of anticancer activity in vivo and in vitro behaviors of liposomes encapsulated iridium(III) complex, J. Biol. Inorg. Chem. 26 (2021) 109–122, https://doi.org/10.1007/s00775-020-01841-9.
[75] H. Zhang, L. Tian, R. Xiao, Y. Zhou, Y. Zhang, J. Hao, Y. Liu, J. Wang, Anticancer effect evaluation in vitro and in vivo of iridium(III) polypyridyl complexes targeting DNA and mitochondria, Bioorg. Chem. 115 (2021) 105290, https://doi.org/10.1016/j.bioorg.2021.105290.
[76] W. Li, X. Wu, H. Liu, C. Shi, Y. Yuan, L. Bai, X. Liao, Y. Zhang, Y. Liu, Enhanced in vitro cytotoxicity and antitumor activity in vivo of iridium(III) complexes liposomes targeting endoplasmic reticulum and mitochondria, J. Inorg. Biochem. 233 (2022) 111868, https://doi.org/10.1016/j.jinorgbio.2022.111868.

Update

Bioorganic Chemistry
Volume 164, Issue , September 2025, Page

DOI: https://doi.org/10.1016/j.bioorg.2025.108810

Bioorganic Chemistry 164 (2025) 108810

Contents lists available at ScienceDirect

Bioorganic Chemistry

journal homepage: www.elsevier.com/locate/bioorg

Corrigendum

Corrigendum to "Designing novel tridentate iridium(III) complexes comprising functionalized benzothiazole ligands to improve anticancer activity by targeting mitochondria" [Bioorg. Chem. 161 (2025) 108507]

Qin Zhou [a,c], Xiao-Bin Zhang [a], An-Li Liu [a,c], Zhi-Gang Niu [a,c,*], Gao-Nan Li [a,c,*], Fa-Biao Yu [b,c]

[a] *Key Laboratory of Electrochemical Energy Storage and Light Energy Conversion Matreials of Haikou City, Key Laboratory of Electrochemical Energy Storage and Energy Conversion of Hainan Province, College of Chemistry and Chemical Engineering, Hainan Normal University, Haikou 571158, China*

[b] *Key Laboratory of Emergency and Trauma, Ministry of Education, Key Laboratory of Haikou Trauma, Key Laboratory of Hainan Trauma and Disaster Rescue, The First Affiliated Hospital, Hainan Medical University, Haikou 571199, China*

[c] *Engineering Research Center for Hainan Bio-Smart Materials and Bio-Medical Devices, Key Laboratory of Hainan Functional Materials and Molecular Imaging, College of Emergency and Trauma, Hainan Medical University, Haikou 571199, China*

We regret that there are Chinese characters in the Fig. 10, it may cause inconvenience to readers from other countries. So I hope the mistake could be corrected in next available issue.

DOI of original article: https://doi.org/10.1016/j.bioorg.2025.108507.

* Corresponding authors at: Key Laboratory of Electrochemical Energy Storage and Light Energy Conversion Matreials of Haikou City, Key Laboratory of Electrochemical Energy Storage and Energy Conversion of Hainan Province, College of Chemistry and Chemical Engineering, Hainan Normal University, Haikou, 571158, China.

E-mail addresses: niuzhigang1982@126.com (Z.-G. Niu), ligaonan2008@163.com (G.-N. Li).

https://doi.org/10.1016/j.bioorg.2025.108810

Available online 5 August 2025

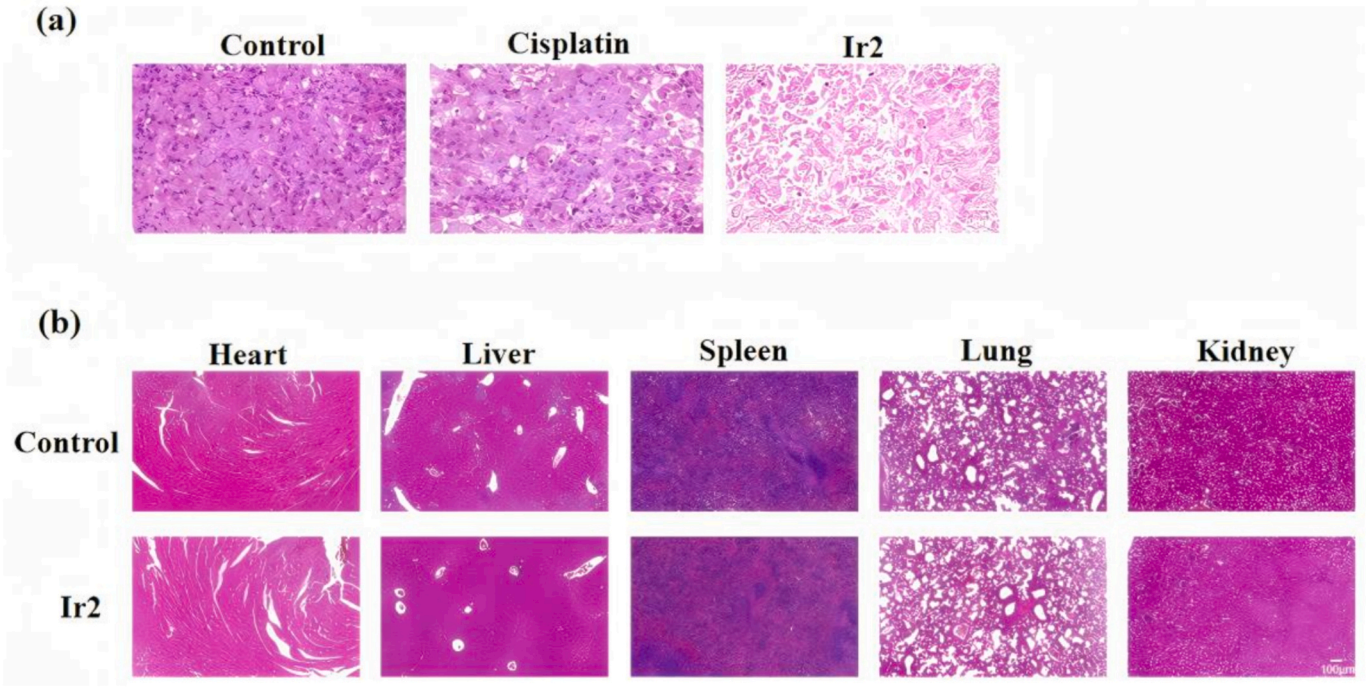

We would like to apologise for any inconvenience caused. And we appreciate greatly any of your help.